Transport in Porous Media (2022) 143:195–223
https://doi.org/10.1007/s11242-022-01792-6

A Multiple-Relaxation-Time Lattice-Boltzmann Analysis for Double-Diffusive Natural Convection in a Cavity with Heating and Diffusing Plate Inside Filled with a Porous Medium

Youssef Dahani[1] · **Mohammed Hasnaoui**[1] · **Abdelkhalek Amahmid**[1] · **Safae Hasnaoui**[1]

Received: 9 November 2021 / Accepted: 20 April 2022 / Published online: 11 May 2022

Abstract
In the present study, a multiple-relaxation-time lattice-Boltzmann method is considered to investigate double-diffusive natural convection in a cavity with heating and diffusing plate inside. The cavity is filled with a porous medium at representative elementary volume scale based on the generalized model. The heated plate is placed horizontally at the center of the cavity with higher temperature and concentration. The horizontal walls of the cavity are assumed to be insulated, no conducting, and impermeable to mass transfer. The vertical walls are kept at low temperature and concentration. The combined effects of buoyancy ratio N ($-5 \leq N \leq 5$), thermal Rayleigh number $\mathrm{Ra_T}$ ($10^4 \leq \mathrm{Ra_T} \leq 10^7$), Darcy number Da ($10^{-6} \leq \mathrm{Da} \leq 10^{-2}$), Lewis number Le ($1 \leq \mathrm{Le} \leq 10$), and porosity of the porous medium ε ($0.4 \leq \varepsilon \leq 0.8$) on double-diffusive natural convection are analyzed numerically. Results are presented in terms of streamlines, isotherms, iso-concentrations, and average Nusselt and Sherwood numbers. Results show that the flow structure, the shape of isotherms, and iso-concentrations are well affected by the control parameters. The heat and mass transfers are promoted by the increase of Darcy number. The effect of the Lewis number on heat transfer is negligible for low Darcy values, but this effect is promoted by increasing Darcy number.

Keywords Multiple-relaxation-time · Double diffusive natural convection · Porous medium · Heated plate · Representative elementary volume

✉ Youssef Dahani
youssef.dahani@uca.ac.ma

Mohammed Hasnaoui
hasnaoui@uca.ac.ma

Abdelkhalek Amahmid
amahmid@uca.ac.ma

Safae Hasnaoui
safae.hasnaoui@edu.uca.ac.ma

[1] Laboratory of Fluid Mechanics and Energetics (LMFE), Unit Affiliated to CNRST (URL-CNRST No 16), Department of Physics, Faculty of Sciences Semlalia, Cadi Ayyad University, BP 2390, Marrakesh, Morocco

1 Introduction

The phenomenon of coupled heat and mass transfer by natural or mixed convection in porous media is generally referred to as fluid flows generated by buoyancy effects due to both temperature and concentration gradients. These two gradients give rise to a non-uniform distribution of the mixture density, which causes convective motion under the effect of gravity. In the case where the volume forces are of thermal origin, natural convection is said to be thermal, it is thermosolutal convection or double-diffusive convection if both thermal and solutal effects coexist.

Double-diffusive convection in a cavity filled with a porous medium is of interest to several manufacturers and researchers because of its involvement in various physical, technological, chemical, and microbiological fields. Among the potential applications are the extraction of geothermal energy, crystal growth to obtain a single crystal from a molten mixture, thermal insulation of buildings, dispersion of pollutants in aquifers and saturated soils, micro-combustion, etc. (Bergman et al. 1986; Carlsson 1985; Coulter and Güçeri 1987; Kaisare and Vlachos 2012; Markham and Rosenberger 1984; Nishimura et al. 1994). Double-diffusive convection in porous media began to attract the attention of researchers after Nield (1968) studied the stability of a horizontal porous layer, heated and salted from below. Using the linear stability analysis, he determined the values of the critical Rayleigh numbers characterizing the onset of stationary convection for different boundary conditions. In a more general study Bennacer et al. (2001) considered a vertical cavity subjected to constant temperatures and concentrations on the vertical walls. The volume forces inducing the flow are assumed to be cooperative. Scale analysis was used in the limit cases of pure thermal ($N \ll 1$) and pure solutal ($N \gg 1$) in the boundary layer regime. They demonstrated that the anisotropic properties of the porous medium significantly affect the rates of heat and mass transfer in the cavity. On their side, Khair and Bejan (1985) considered the phenomenon of thermosolutal convection occurring near a vertical plate immersed in a porous medium saturated with a fluid. Using a scale analysis, they have identified four possible convection regimes according to the values of the buoyancy ratio N and the Lewis number Le.

Several computational methods have been used to study double-diffusive convection in porous media. Conventional techniques like finite element method (FEM) (Nithiarasu et al. 1996, 1997b), finite volume method (FVM) (Mohamad et al. 2004; Tasmin et al. 2021), and finite-difference method (FDM) (Chamkha and Al-Naser 2001) have been applied to deal with such problems. The lattice Boltzmann method (LBM) has been used extensively as a powerful numerical tool to simulate complex fluid flows and model the physics of complex fluids (Benzi et al. 1992; Chen and Doolen 1998; Gong and Cheng 2013; Ma et al. 2014; Ma and Chen 2014; Molla et al. 2018). Generally, a distinction is made between two classes of LBM models, which are used for the simulation of flows in porous media: the representative elementary volume (REV) scale method (Liu et al. 2014; Seta et al. 2006) and the pore-scale method (Kang et al. 2007; Tang et al. 2005). The representative elementary volume (REV) scale approach is widely adopted to study heat and mass transfer because it statistically allows to determine the macroscopic quantities. In fact, in the REV scale LBM, the effect of the porous media has been considered by adding an extra term to the standard LB equation based on different models: the Darcy model, the Brinkman-extended Darcy model, and the Forchheimer-extended Darcy model (Kang et al. 2002). It is admitted that the Brinkman–Forchheimer-extended Darcy model, which is called the generalized model, overcomes some limitations of the Darcy

model, the Brinkman-extended Darcy model, and the Forchheimer-extended Darcy model (Guo and Zhao 2002). The Darcy equation including Brinkman and Forchheimer's terms to account for viscous and inertia effects was used in the momentum equation for the first time by Chen and Chen (1993) while considering the double-diffusive fingering convection in a porous medium. A numerical mixed Galerkin-finite difference method was adopted to predict the limits of stabilities delimiting the different flow regimes as a function of the thermal and solutal Rayleigh numbers. Karimi-Fard et al. (1997) conducted a numerical analysis of double-diffusive convection in a square cavity filled with a porous medium for various pertinent controlling parameters. Non-Darcian effects were analyzed by investigating the average heat and mass transfer rates. The results of this investigation show that the inertial and boundary effects have a significant effect on double-diffusive convection.

Combustion is one of the applications where the phenomenon of double-diffusive convection is ubiquitous. In a combustion environment within an inert porous medium, the heat transfer and mixing of the reacting species are intensified, which leads to a combustion mode having different characteristics compared to free premixed combustion, such as a considerable reduction in polluting species (Mohamad 2005).

To the best of the authors' knowledge, no attention has been paid to the problem of double-diffusive convection flow in a porous enclosure with an inner heating and diffusing thin plate placed inside [case of the low-pressure flat flame (El Bakali et al. 2012; de Ferrières et al. 2013)]. Very schematically, it imitates the combustion of an object located in the center of a room or in a porous burner (Howell et al. 1996; Mujeebu et al. 2009, 2010; Trimis and Durst 1996; Viskanta 2011; Wood and Harris 2008). The release of heat and the injection of active gases generate a confined floating plume due to the combined effects of thermal and concentration gradients.

The present study focuses on the analysis of double-diffusive convection flow in a square enclosure filled with a porous medium with inner heating and diffusing horizontal thin plate centrally located using multiple-relaxation-time (MRT) lattice-Boltzmann method (LBM) at the REV scale based on the generalized model. Moreover, the effect of a wide range of the pertinent parameters such as thermal Rayleigh number ($\mathrm{Ra_T}$), Lewis number (Le), Buoyancy ratio (N), Darcy number (Da) and porosity of the medium (ε) is considered in the present study to investigate the impact of these parameters on heat and mass transfer characteristics.

2 Mathematical Model

The studied configuration is a two-dimensional square enclosure [low-pressure burner sketched in Fig. 1a (Mercier et al. 2020)] of height and width H, filled with an inert porous medium. The latter is provided with a heated plate of length $h = \frac{L}{2}$, placed horizontally so that its center and that of the cavity coincide as shown in Fig. 1b. The plate is maintained at a higher temperature T_h and concentration C'_h. The horizontal walls are assumed insulated, non-conducting, and impermeable to mass transfer. The vertical walls are kept at low temperature and concentration ($T_L < T_h$ and $C'_L < C'_h$). The fluid that saturates the enclosure is Newtonian and incompressible. The porous medium is supposed isotropic, homogeneous, and in thermodynamic equilibrium with the fluid. The effects of Soret and Dufour are neglected in the present study. The thermophysical properties of the fluid are assumed constant, except the density variation in the buoyancy force, which obeys the Boussinesq

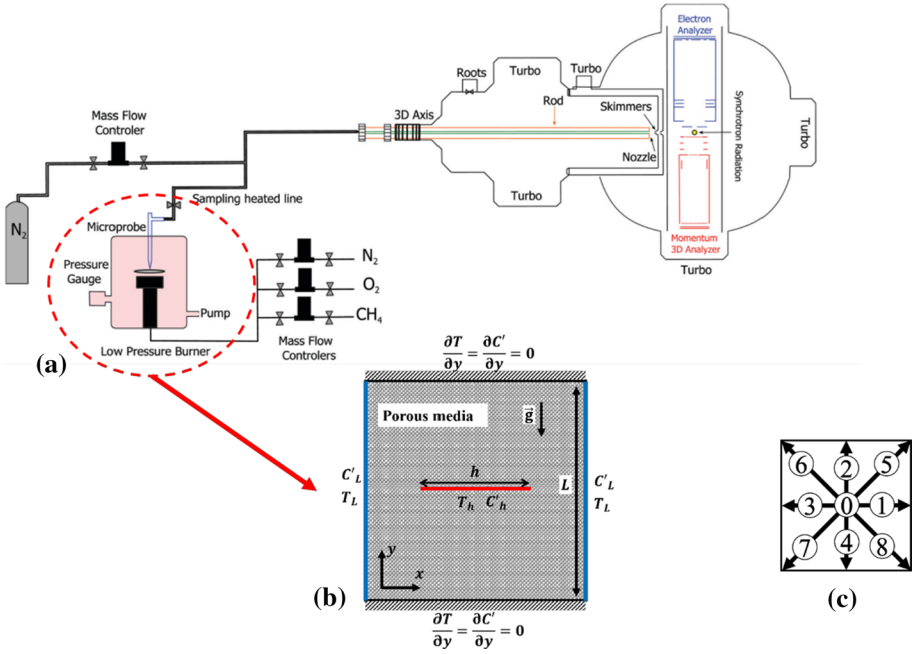

Fig. 1 **a** A schematic representation of the low-pressure flat flame growth apparatus (Mercier et al. 2020); **b** schematic of the studied configuration; **c** schematic view of the two-dimensional nine-velocity D_2Q_9 model

approximation. Therefore, the fluid density varies with temperature and concentration according to the linearized state equation (Bejan 2013):

$$\rho = \rho_0\left(1 - \beta_T\left(T - T_0\right) - \beta_C\left(C' - C'_0\right)\right) \tag{1}$$

where ρ_0 is the fluid density at the reference temperature $T' = T_0$, and concentration $C' = C'_0$, and β_T and β_C are the thermal and concentration expansion coefficients, respectively. They are expressed as follows (Bejan 2013):

$$\beta_T = -\frac{1}{\rho_0}\left(\frac{\partial \rho}{\partial T}\right)_{P,C} \quad \beta_C = -\frac{1}{\rho_0}\left(\frac{\partial \rho}{\partial C'}\right)_{P,T} \tag{2}$$

The governing equations, based on the Darcy–Brinkman–Forchheimer extended model, can be expressed as follows (Nithiarasu et al. 1997a):

$$\nabla \cdot \boldsymbol{u} = 0 \tag{3}$$

$$\frac{\partial u}{\partial t'} + (\boldsymbol{u} \cdot \nabla)\left(\frac{\boldsymbol{u}}{\varepsilon}\right) = -\frac{1}{\rho_0}\nabla(\varepsilon p) + \nu\nabla^2\boldsymbol{u} + \boldsymbol{F} \tag{4}$$

$$\frac{\partial T}{\partial t'} + \nabla \cdot (\boldsymbol{u}T) = \alpha\nabla^2 T \tag{5}$$

$$\frac{\partial C'}{\partial t'} + \nabla \cdot \left(\boldsymbol{u}C'\right) = D\nabla^2 C' \tag{6}$$

where $\boldsymbol{u} = (u, v)^{\mathrm{T}}$ is the velocity vector, p is pressure, T is the local temperature, C' is the concentration, ν is the fluid kinematic viscosity, α its thermal diffusivity, D is the mass diffusivity of the saturated porous medium, ε is the porosity, and $\boldsymbol{F}$ is the total body force induced by the porous matrix and other external forces, which is given by the following expression (Ergun 1952):

$$\boldsymbol{F} = -\frac{\varepsilon\nu}{K}\boldsymbol{u} - \frac{\varepsilon F_{\varepsilon}}{\sqrt{K}}|\boldsymbol{u}|\boldsymbol{u} + \varepsilon\boldsymbol{G} \tag{7}$$

where K is the permeability and $|\boldsymbol{u}| = \sqrt{u^2 + v^2}$. The buoyancy force $\boldsymbol{G}$ is given by (Liu and He 2018):

$$\boldsymbol{G} = g\beta_T\left(T - T_0\right)\boldsymbol{j} + g\beta_C\left(C' - C'_0\right)\boldsymbol{j} \tag{8}$$

where g is the gravitational acceleration, $T_0 = \frac{T_h+T_L}{2}$ and $C'_0 = \frac{C'_h+C'_L}{2}$ are the reference temperature and concentration, respectively, $\boldsymbol{j}$ is the unit vector in the y-direction.

Based on Ergun's experimental relation (Ergun 1952), the inertial coefficient (Forchheimer coefficient) of the porous medium F_{ε} can be expressed as (Vafai 1984):

$$F_{\varepsilon} = \frac{1.75}{\sqrt{150\varepsilon^3}} \tag{9}$$

The following dimensionless variables are obtained using appropriate scales of length, velocity, temperature, and concentration:

$$(X, Y) = \left(\frac{x}{H}, \frac{y}{H}\right), \quad (U, V) = \left(\frac{uH}{\alpha}, \frac{vH}{\alpha}\right), \quad \theta = \frac{T - T_0}{T_h - T_L} \text{ and } C = \frac{C' - C'_0}{C'_h - C'_L} \tag{10}$$

The system is governed by Eqs. (3)–(6) characterized by several dimensionless parameters, which are the thermal Rayleigh number $\mathrm{Ra_T}$, the Prandtl number Pr, the Lewis number Le, the buoyancy ratio N, and the Darcy number Da, defined as follows:

$$\begin{aligned} \mathrm{Ra_T} &= \frac{\mathrm{g}\beta_T\left(T_h - T_L\right)H^3}{\alpha\nu} \quad \mathrm{Pr} = \frac{\nu}{\alpha} \quad \mathrm{Le} = \frac{\alpha}{D} \\ N &= \frac{\beta_C\left(C'_h - C'_L\right)}{\beta_T\left(T_h - T_L\right)} \quad \mathrm{Da} = \frac{K}{H^2} \end{aligned} \tag{11}$$

The boundary conditions, expressed in terms of dimensionless variables, are such that:

$$U = V = 0, \theta = \theta_L = 0, C = C_L = 0 \text{ at } X = 0 \text{ and } X = 1 \tag{12}$$

$$U = V = 0, \frac{\partial\theta}{\partial Y} = \frac{\partial C}{\partial Y} = 0 \text{ at } Y = 0 \text{ and } Y = 1 \tag{13}$$

$$U = V = 0, \theta = \theta_h = 1, C = C_h = 1 \text{ at the plate} \tag{14}$$

The dimensionless stream function is calculated from the following relations:

$$U = \frac{\partial \psi}{\partial Y} \quad V = -\frac{\partial \psi}{\partial X} \tag{15}$$

The average heat and mass fluxes at the vertical walls are represented in dimensionless forms by the average Nusselt and Sherwood numbers:

$$\mathrm{Nu} = \int_0^1 \left(\frac{\partial \theta}{\partial X}\right)_{X=0} \mathrm{d}Y + \int_0^1 \left(\frac{\partial \theta}{\partial X}\right)_{X=1} \mathrm{d}Y \tag{16}$$

$$\mathrm{Sh} = \int_0^1 \left(\frac{\partial C}{\partial X}\right)_{X=0} \mathrm{d}Y + \int_0^1 \left(\frac{\partial C}{\partial X}\right)_{X=1} \mathrm{d}Y \tag{17}$$

The convergence criterion used to estimate the achievement of the steady-state solution was based on the following local criterion:

$$\left| \frac{\phi_{ij}^{n+1} - \phi_{i,j}^{n}}{\phi_{i,j}^{n}} \right| < 10^{-7} \tag{18}$$

where n indicates the time level and ϕ represents any of the dimensionless variables θ, C, U or V.

3 Numerical Method

3.1 MRT-LB Model for Double-Diffusive Convection in Porous Media

3.1.1 MRT-LB Equation for the Flow Field

The D_2Q_9 lattice velocity model (Fig. 1c) is used in this study, and the corresponding discrete velocity set is given as:

$$\boldsymbol{c}_k = \left(c_{kx}, c_{ky}\right) = \begin{cases} (0,0), & k = 0 \\ c\left(\cos\left[(k-1)\frac{\pi}{2}\right], \sin\left[(k-1)\frac{\pi}{2}\right]\right), & k = 1,2,3,4 \\ \sqrt{2}c\left(\cos\left[(2k-9)\frac{\pi}{4}\right], \sin\left[(2k-9)\frac{\pi}{4}\right]\right), & k = 5,6,7,8 \end{cases} \tag{19}$$

where $c = \frac{\Delta x}{\Delta t} = 1$ is the lattice speed. Δx and Δt are the lattice spacing and the time step, respectively, with $\Delta x = \Delta t = 1$.

Different works using the SRT-LB to deal with porous media flows at REV scale (Gao et al. 2014; Guo and Zhao 2002; Spaid and Phelan 1997; Wang et al. 2016) are available in the literature. The MRT lattice-Boltzmann model is chosen as the flow (Eq. 4), temperature (Eq. 5) and concentration (Eq. 6) fields solvers. The MRT lattice-Boltzmann equation with a force term can be expressed as:

$$\boldsymbol{f}\left(\boldsymbol{r} + \boldsymbol{c}_k \Delta t, t + \Delta t\right) - \boldsymbol{f}(\boldsymbol{r}, t) = -\boldsymbol{M}^{-1}\boldsymbol{S}_f(\boldsymbol{m}(\boldsymbol{r}, t) - \boldsymbol{m}^{\mathrm{eq}}(\boldsymbol{r}, t)) + \boldsymbol{M}^{-1}\left(\boldsymbol{I} - \frac{1}{2}\boldsymbol{S}_f\right)\Delta t \boldsymbol{F}(\boldsymbol{r}, t) \tag{20}$$

where the above quantities are obtained as follows:

$$\boldsymbol{f}(\boldsymbol{r},t) = \left(f_0(\boldsymbol{r},t), f_1(\boldsymbol{r},t), \ldots, f_8(\boldsymbol{r},t)\right)^{\mathrm{T}} \tag{21}$$

$$\boldsymbol{m}(\boldsymbol{r},t) = \boldsymbol{M}\boldsymbol{f} = \left(m_0(\boldsymbol{r},t), m_1(\boldsymbol{r},t), \ldots, m_8(\boldsymbol{r},t)\right)^{\mathrm{T}} \tag{22}$$

$$\boldsymbol{m}^{\mathrm{eq}}(\boldsymbol{r},t) = \left(m_0^{\mathrm{eq}}(\boldsymbol{r},t), m_1^{\mathrm{eq}}(\boldsymbol{r},t), \ldots, m_8^{\mathrm{eq}}(\boldsymbol{r},t)\right)^{\mathrm{T}} \tag{23}$$

$$\boldsymbol{F}(\boldsymbol{r},t) = \left(F_0(\boldsymbol{r},t), F_1(\boldsymbol{r},t), \ldots, F_8(\boldsymbol{r},t)\right)^{T} \tag{24}$$

In Eq. (21), $\left\{f_k(\boldsymbol{r},t)\middle|k=0,\ldots,8\right\}$ are the density distribution functions for the discrete velocities $\left\{\boldsymbol{c}_k\middle|k=0,\ldots,8\right\}$. $\left\{m_k\middle|k=0,\ldots,8\right\}$ and $\left\{m_k^{\mathrm{eq}}\middle|k=0,\ldots,8\right\}$ are the moments of the distribution functions, and the corresponding equilibrium moments. In Eq. (24), $\left\{F_k\middle|k=0,\ldots,8\right\}$ are the discrete force terms in the moment space. The matrices $\boldsymbol{I}$ and $\boldsymbol{M}$ are, respectively, the unit matrix and the orthogonal transformation matrix that can be constructed as (Liu et al. 2014):

$$\boldsymbol{M} = \begin{pmatrix} 1 & 1 & 1 & 1 & 1 & 1 & 1 & 1 & 1 \\ -4 & -1 & -1 & -1 & -1 & 2 & 2 & 2 & 2 \\ 4 & -2 & -2 & -2 & -2 & 1 & 1 & 1 & 1 \\ 0 & 1 & 0 & -1 & 0 & 1 & -1 & -1 & 1 \\ 0 & -2 & 0 & 2 & 0 & 1 & -1 & -1 & 1 \\ 0 & 0 & 1 & 0 & -1 & 1 & 1 & -1 & -1 \\ 0 & 0 & -2 & 0 & 2 & 1 & 1 & -1 & -1 \\ 0 & 1 & -1 & 1 & -1 & 0 & 0 & 0 & 0 \\ 0 & 0 & 0 & 0 & 0 & 1 & -1 & 1 & -1 \end{pmatrix} \tag{25}$$

$$\boldsymbol{S}_f = \mathrm{diag}\left(s_0, s_1, \ldots, s_8\right) \tag{26}$$

In Eq. (26), $\boldsymbol{S}_f$ is the diagonal relaxation matrix where $s_0 = s_3 = s_5 = 0$. as they correspond to the conserved moments during the collision phase. For the sake of stability s_1, s_2, s_4 and s_6 are chosen slightly greater than unity. The fluid kinematic viscosity is correlated to the relaxation rates s_7 and s_8 through the Chapman–Enskog expansion analysis (Dahani et al. 2022; Hasnaoui et al. 2021) as folws:

$$\nu = \frac{1}{3}\left(\frac{1}{\mathrm{s}_8} - \frac{1}{2}\right) = \frac{1}{3}\left(\frac{1}{\mathrm{s}_7} - \frac{1}{2}\right) \tag{27}$$

To ensure that the code works in a near-incompressible regime, the Mach number Ma should be less than 0.3. In this work, the Mach number was selected to be 0.1. By fixing the thermal Rayleigh number, the Prandtl number, and the Mach number, the viscosity can be calculated by the following expression:

$$\nu = \mathrm{Ma} \cdot m \cdot \sqrt{\frac{\mathrm{Pr}}{3\mathrm{Ra}_{\mathrm{T}}}} \tag{28}$$

where m is the lattice number.

For the present MRT lattice-Boltzmann model, the key point is the choice of the appropriate equilibrium moments and discrete force term in the moment space. Here, the following equilibrium moments $\boldsymbol{m}_k^{eq}$ are selected (Liu et al. 2014):

$$\boldsymbol{m}_k^{\mathrm{eq}} = \left(\rho, -2\rho + \frac{3\rho|\boldsymbol{u}^2|}{\varepsilon}, \rho - \frac{3\rho|\boldsymbol{u}^2|}{\varepsilon}, \rho u, -\rho u, \rho v, -\rho v, \frac{\rho\left(u^2 - v^2\right)}{\varepsilon}, \frac{\rho uv}{\varepsilon}\right)^{\mathrm{T}} \tag{29}$$

The total body force $\boldsymbol{F}$ is obtained by adding a forcing term to the collision step in the moment space with the fluid velocity. Thus, the components of the forcing term $\left\{F_k | k = 0, \ldots, 8\right\}$ in the moment space are given explicitly as (Liu et al. 2014):

$$\begin{aligned} &F_0 = 0, \quad F_1 = \frac{6\rho\left(uF_x + vF_y\right)}{\varepsilon}, \quad F_2 = -\frac{6\rho\left(uF_x + vF_y\right)}{\varepsilon}, \quad F_3 = \rho F_x, \\ &F_4 = -\rho F_x, \quad F_5 = \rho F_y, \quad F_6 = -\rho F_y, \\ &F_7 = \frac{2\rho\left(uF_x - vF_y\right)}{\varepsilon}, \quad F_8 = \frac{\rho\left(uF_y + vF_x\right)}{\varepsilon}, \end{aligned} \tag{30}$$

where F_x and F_y are obtained as:

$$\begin{aligned} F_x &= -\frac{\varepsilon\nu}{K}u - \frac{1.75}{\sqrt{150\varepsilon^3 K}}u\sqrt{u^2 + v^2} \\ F_y &= -\frac{\varepsilon\nu}{K}v - \frac{1.75}{\sqrt{150\varepsilon^3 K}}v\sqrt{u^2 + v^2} + \varepsilon g\beta_T\left(\left(\theta - \theta_0\right) + N\left(C - C_0\right)\right) \end{aligned} \tag{31}$$

Then, the macroscopic density ρ and velocity $\boldsymbol{u}$ are given by:

$$\rho(\boldsymbol{r}, t) = \sum_{k=0}^{8} f_k(\boldsymbol{r}, t) \tag{32}$$

$$\boldsymbol{u}(\boldsymbol{r}, t) = \frac{\boldsymbol{W}}{l_0 + \sqrt{l_0^2 + l_1|\boldsymbol{W}|}} \tag{33}$$

where $\boldsymbol{W}$ is a temporal velocity calculated by the following expression:

$$\boldsymbol{W}(\boldsymbol{r}, t) = \sum_{k=0}^{8} \frac{\boldsymbol{c}_k f_k(\boldsymbol{r}, t)}{\rho(\boldsymbol{r}, t)} + \frac{\varepsilon \boldsymbol{G}}{2} \tag{34}$$

The two parameters l_0 and l_1 in Eq. (33) are given by:

$$l_0 = \frac{1}{2}\left(1 + \frac{\varepsilon\nu}{2K}\right) \quad l_1 = \frac{\varepsilon}{2}\frac{F_\varepsilon}{\sqrt{K}} \tag{35}$$

3.1.2 MRT Lattice-Boltzmann Method for Temperature and Concentration Fields

For double-diffusive convection in porous media, the temperature and concentration fields.

are governed by Eqs. (5) and (6). These last equations were solved separately by MRT-LB equations based on the two-dimensional D_2Q_5 model. The MRT-LB equations for the temperature and concentration fields are described by the distribution functions $\boldsymbol{g}$ (for temperature) and $\boldsymbol{h}$ (for concentration) expressed by the following equations:

$$\boldsymbol{g}\left(\boldsymbol{r}+\boldsymbol{c}_k\Delta t, t+\Delta t\right)-\boldsymbol{g}(\boldsymbol{r},t)=-\boldsymbol{N}^{-1}\boldsymbol{S}_g\left(\boldsymbol{n}_g(\boldsymbol{r},t)-\boldsymbol{n}_g^{\mathrm{eq}}(\boldsymbol{r},t)\right) \tag{36}$$

$$\boldsymbol{h}\left(\boldsymbol{r}+\boldsymbol{c}_k\Delta t, t+\Delta t\right)-\boldsymbol{h}(\boldsymbol{r},t)=-\boldsymbol{N}^{-1}\boldsymbol{S}_h\left(\boldsymbol{n}_h(\boldsymbol{r},t)-\boldsymbol{n}_h^{\mathrm{eq}}(\boldsymbol{r},t)\right) \tag{37}$$

where the above notations denote:

$$\boldsymbol{g}(\boldsymbol{r},t)=\left(g_0(\boldsymbol{r},t), g_1(\boldsymbol{r},t), \ldots, g_4(\boldsymbol{r},t)\right)^{\mathrm{T}} \tag{38}$$

$$\boldsymbol{n}_g(\boldsymbol{r},t)=\boldsymbol{N}\boldsymbol{g}=\left(n_{g0}(\boldsymbol{r},t), n_{g1}(\boldsymbol{r},t), \ldots, n_{g4}(\boldsymbol{r},t)\right)^{\mathrm{T}} \tag{39}$$

$$\boldsymbol{n}_g^{\mathrm{eq}}(\boldsymbol{r},t)=\left(n_{g0}^{\mathrm{eq}}(\boldsymbol{r},t), n_{g1}^{\mathrm{eq}}(\boldsymbol{r},t), \ldots, n_{g4}^{\mathrm{eq}}(\boldsymbol{r},t)\right)^{\mathrm{T}} \tag{40}$$

$$\boldsymbol{h}(\boldsymbol{r},t)=\left(h_0(\boldsymbol{r},t), h_1(\boldsymbol{r},t), \ldots, h_4(\boldsymbol{r},t)\right)^{\mathrm{T}} \tag{41}$$

$$\boldsymbol{n}_h(\boldsymbol{r},t)=\boldsymbol{N}\boldsymbol{h}=\left(n_{h0}(\boldsymbol{r},t), n_{h1}(\boldsymbol{r},t), \ldots, n_{h4}(\boldsymbol{r},t)\right)^{\mathrm{T}} \tag{42}$$

$$\boldsymbol{n}_h^{\mathrm{eq}}(\boldsymbol{r},t)=\left(n_{h0}^{\mathrm{eq}}(\boldsymbol{r},t), n_{h1}^{\mathrm{eq}}(\boldsymbol{r},t), \ldots, n_{h4}^{\mathrm{eq}}(\boldsymbol{r},t)\right)^{\mathrm{T}} \tag{43}$$

where $\left\{ g_k(\boldsymbol{r},t)\middle| k=0,\ldots,4\right\}$ and $\left\{ h_k(\boldsymbol{r},t)\middle| k=0,\ldots,4\right\}$ are, respectively, the discrete temperature and concentration distributions functions for the discrete velocities $\left\{\boldsymbol{c}_k\middle| k=0,\ldots,4\right\}$. The discrete parameters $\left\{ n_{gk}\middle| k=0,\ldots,4\right\}$, $\left\{ n_{gk}^{\mathrm{eq}}\middle| k=0,\ldots,4\right\}$, $\left\{ n_{hk}\middle| k=0,\ldots,4\right\}$ and $\left\{ n_{hk}^{\mathrm{eq}}\middle| k=0,\ldots,4\right\}$ are the moments and their corresponding equilibrium moments, respectively, for temperature and concentration distributions functions. The matrix $\boldsymbol{N}$ is an orthogonal transformation matrix constructed as follows (Liu et al. 2014):

$$N=\begin{pmatrix} 1 & 1 & 1 & 1 & 1 \\ 0 & 1 & 0 & -1 & 0 \\ 0 & 0 & 1 & 0 & -1 \\ -4 & 1 & 1 & 1 & 1 \\ 0 & 1 & -1 & 1 & -1 \end{pmatrix} \tag{44}$$

$$\boldsymbol{S}_g=\mathrm{diag}\left(s_{g0}, s_{g1}, \ldots, s_{g4}\right) \tag{45}$$

$$\boldsymbol{S}_h=\mathrm{diag}\left(s_{h0}, s_{h1}, \ldots, s_{h4}\right) \tag{46}$$

In Eqs. (45) and (46), $\boldsymbol{S}_g$ and $\boldsymbol{S}_h$ are the diagonal relaxation matrix where $s_{g0}=s_{g3}=s_{g4}=1$, $s_{h0}=s_{h3}=s_{h4}=1$, $\mathrm{s}_{g1}=\mathrm{s}_{g2}=\left(\frac{10\alpha}{4+a}+0.5\right)^{-1}$ and $\mathrm{s}_{h1}=\mathrm{s}_{h2}=\left(\frac{10D}{4+a}+0.5\right)^{-1}$. The con-

stant a was set to -2 in order to have the same sound speed in both D_2Q_9 and D_2Q_5 models.

The equilibrium moment vectors $\boldsymbol{n}_g^{\mathrm{eq}}$ and $\boldsymbol{n}_h^{\mathrm{eq}}$ are chosen as follows:

$$\boldsymbol{N}_{gk}^{\mathrm{eq}} = (\theta, u\theta, v\theta, a\theta, 0)^{\mathrm{T}} \tag{47}$$

$$\boldsymbol{N}_{hk}^{\mathrm{eq}} = (C, uC, vC, aC, 0)^{\mathrm{T}} \tag{48}$$

The macroscopic temperature and concentration can be obtained via the following relations:

$$\theta(\boldsymbol{r}, t) = \sum_{k=0}^{4} g_k(\boldsymbol{r}, t) \tag{49}$$

$$C(\boldsymbol{r}, t) = \sum_{k=0}^{4} h_k(\boldsymbol{r}, t) \tag{50}$$

3.2 Boundary Conditions

The boundary conditions associated with this problem are characterized by the non-slip of the fluid particles on the rigid boundaries and the impermeability of the latter. Hence, classical bounce-back boundary conditions were applied on the walls of the cavity. The functions oriented to the exterior of the cavity are known since they have been determined in the streaming step. After the collision, all the functions oriented to the interior of the cavity are unknown, they are deduced by using the values of the functions oriented (mirror) to the exterior. For the bottom and the top walls, the following conditions were used for temperature and concentration:

$$g_{k,0} = \frac{4g_{k,1} - g_{k,2}}{3}, k = 0, \ldots, 4 \quad g_{k,m} = \frac{4g_{k,m-1} - g_{k,m-2}}{3}, k = 0, \ldots, 4 \tag{51}$$

$$h_{k,0} = \frac{4h_{k,1} - h_{k,2}}{3}, k = 0, \ldots, 4 \quad h_{k,m} = \frac{4h_{k,m-1} - h_{k,m-2}}{3}, k = 0, \ldots, 4 \tag{52}$$

For the left and right walls, the following conditions were used for temperature and concentration:

$$g_{1,0} = \frac{2\theta_L\left(1 + \frac{a}{4}\right)}{5} - g_{3,0} \quad g_{3,n} = \frac{2\theta_L\left(1 + \frac{a}{4}\right)}{5} - g_{1,n} \tag{53}$$

$$h_{1,0} = \frac{2C_L\left(1 + \frac{a}{4}\right)}{5} - h_{3,0} \quad h_{3,n} = \frac{2C_L\left(1 + \frac{a}{4}\right)}{5} - h_{1,n} \tag{54}$$

For the top, the bottom, the left and the right sides of the thin plate, the following conditions were used for temperature and concentration:

$$
\begin{aligned}
g_{2,\text{top}} &= \frac{2\theta_h\left(1+\frac{a}{4}\right)}{5} - g_{4,\text{top}} \quad g_{4,\text{bottom}} = \frac{2\theta_h\left(1+\frac{a}{4}\right)}{5} - g_{2,\text{bottom}} \\
g_{3,\text{left}} &= \frac{2\theta_h\left(1+\frac{a}{4}\right)}{5} - g_{1,\text{left}} \quad g_{1,\text{right}} = \frac{2\theta_h\left(1+\frac{a}{4}\right)}{5} - g_{3,\text{right}}
\end{aligned} \tag{55}
$$

$$
\begin{aligned}
h_{2,\text{top}} &= \frac{2C_h\left(1+\frac{a}{4}\right)}{5} - h_{4,\text{top}} \quad h_{4,\text{bottom}} = \frac{2C_h\left(1+\frac{a}{4}\right)}{5} - h_{2,\text{bottom}} \\
h_{3,\text{left}} &= \frac{2C_h\left(1+\frac{a}{4}\right)}{5} - h_{1,\text{left}} \quad h_{1,\text{right}} = \frac{2C_h\left(1+\frac{a}{4}\right)}{5} - h_{3,\text{right}}
\end{aligned} \tag{56}
$$

3.3 Numerical Validation and Grid Size Effect

The numerical code was validated in the case of natural convection in a cavity with a heated plate inside (Saravanan and Sivaraj 2013) and in the case of pure thermal natural convection in a porous cavity against numerical (Chen et al. 2009; Molla et al. 2018; Nithiarasu et al. 1997a) and experimental (Molla et al. 2018; Sathe et al. 1987) data and in the case of double-diffusive convection around a heated cylinder in a closed cavity filled with porous media (Xu et al. 2017). The comparative results are presented in Fig. 2 (natural convection in a cavity with a heated plate inside), Tables 1 and 2 (pure thermal natural

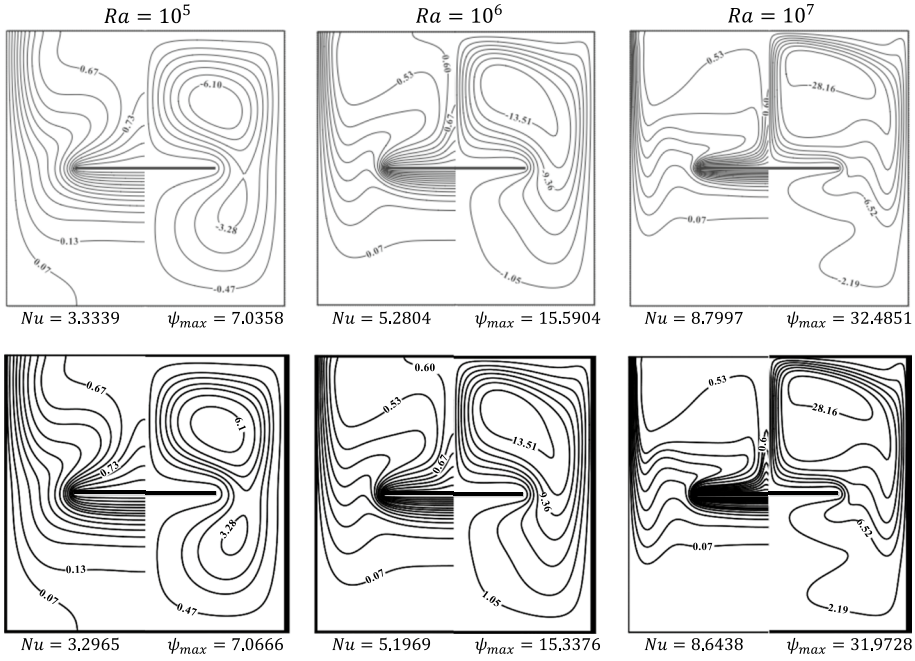

Fig. 2 Comparison between our results (bottom) and those of Saravanan and Sivaraj (Saravanan and Sivaraj 2013) (top)

Table 1 Validation in terms of average Nusselt number with previous studies

	Da	Ra	Nithiarasu et al. (1997a)	Chen et al. (2009)	Molla et al. (2018)	MRT LB
$\epsilon = 0.4$	10^{-2}	10^3	1.01	1.01	1.0197	1.0076
		10^4	1.408	1.362	1.3546	1.3606
		10^5	2.983	2.990	3.0293	2.9969
	10^{-4}	10^5	1.067	1.064	1.0681	1.0659
		10^6	2.55	2.60	2.6263	2.6093
		10^7	7.81	7.86	7.7831	7.8429
$\epsilon = 0.6$	10^{-2}	10^3	1.015	1.012	1.0240	1.0118
		10^4	1.530	1.500	1.5079	1.4916
		10^5	3.555	3.445	3.4855	3.4529
	10^{-4}	10^5	1.071	1.070	1.0914	1.0695
		10^6	2.725	2.714	2.7418	2.7183
		10^7	8.1836	8.648	8.1243	8.6620

Table 2 Experimental validation in terms of average Nusselt number

Da	Ra	Pr	Experimental (Sathe et al. 1987)	Molla et al. (2018)	MRT LB
1.048×10^{-4}	1.72×10^6	6.30	2.75	2.78	2.7379
	2.47×10^6	6.11	3.30	3.24	3.2713
	3.04×10^6	6.07	3.70	3.64	3.6837
3.672×10^{-4}	1.02×10^6	6.16	3.35	3.35	3.3335
	1.67×10^6	6.18	4.07	4.16	4.1298
	2.38×10^6	6.22	4.69	4.63	4.6410

convection in a porous cavity), Fig. 3 and Table 3 (double-diffusive natural convection in a porous medium). The qualitative and quantitative results presented in Fig. 2 show that our code reproduces satisfactorily the results reported in Saravanan and Sivaraj (2013) with a maximum deviation of 1.6%. The results presented in Tables 1 and 2 show an excellent agreement between the MRT-LBM results, and those reported in Chen et al. (2009), Molla et al. (2018), Nithiarasu et al. (1997a) and Sathe et al. (1987). Also, the comparative results presented in Fig. 3 in terms of streamlines, isotherms, and iso-concentrations, and the quantitative results presented in Table 3 in terms of Nusselt and Sherwood numbers show that our code reproduces satisfactorily the results reported in Xu et al. (2017) with a maximum deviation of 4.2%.

A uniform grid of 200×200 was used in the present study. The choice of this grid was based on several preliminary tests performed to assess the sensitivity of the results vis-a-vis the variations of the mesh. A summary of representative results is presented in terms of ψ_{max}, Nu and Sh for various grids and various Darcy numbers for $\epsilon = 0.4$ in Table 4 for $Ra_T = 10^5$, Le = 2 and $N = 5$ and in Table 4(a) for $Ra_T = 10^7$, Le = 10 and $N = 1$. The analysis of the results presented in Table 4(b) shows that, by refining the retained grid to

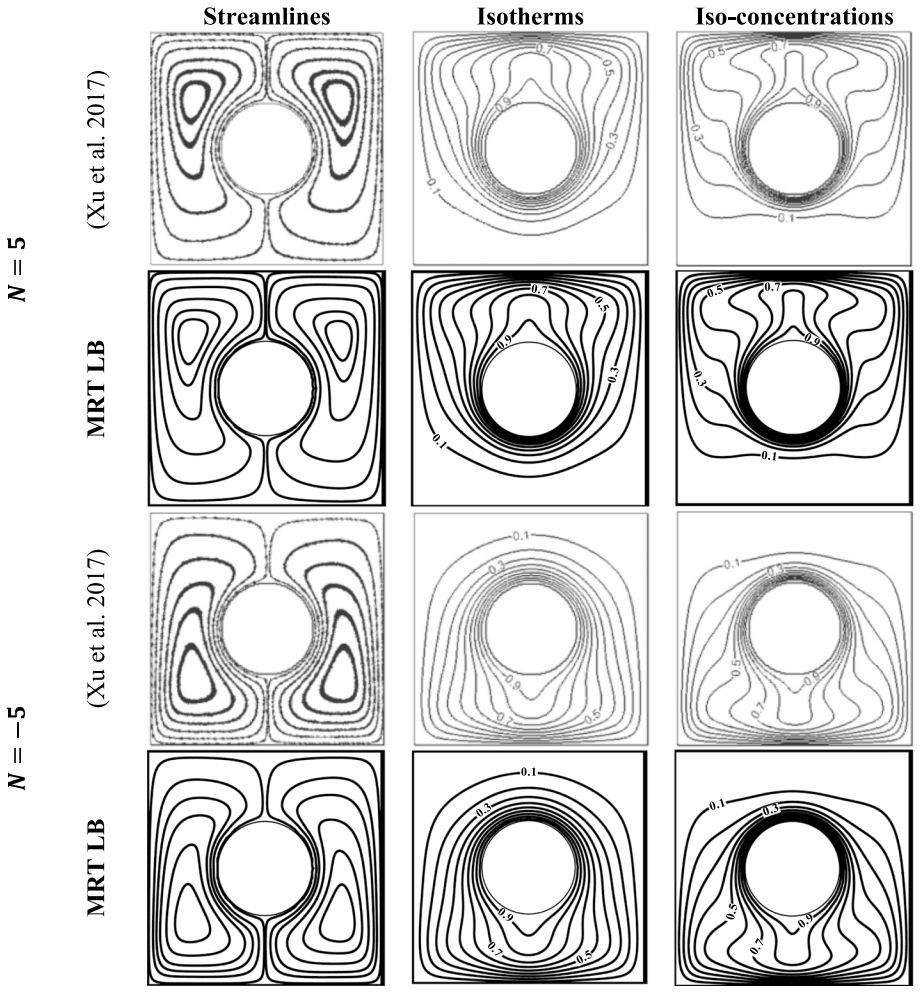

Fig. 3 Comparison between our results and those of Xu et al. (2017) for $Ra_T = 10^5$, Le = 2, and $Da = 10^{-3}$

Table 3 Validation of the numerical code versus published results of Xu et al. (2017) for $Ra_T = 10^5$ and $Da = 10^{-3}$

	$N = 5$				$N = -5$			
	Le = 0.5		Le = 2		Le = 10		Le = 2	
	Nu	Sh	Nu	Sh	Nu	Sh	Nu	Sh
Xu et al. (2017)	6.532	4.439	5.522	7.530	3.929	12.622	4.593	6.776
MRT LB	6.311	4.445	5.332	7.636	4.045	12.645	4.560	6.487
Deviation	3.4%	0.13%	3.4%	1.4%	2.9%	0.18%	0.7%	4.2%

Table 4 Grid sensitivity analysis for various Darcy numbers, (a) $Ra_T = 10^5$, $\varepsilon = 0.4$, Le = 2, and $N = 5$, (b) $Ra_T = 10^7$, $\varepsilon = 0.4$ Le = 10, and $N = 1$

	Grid size	ψ_{max}	Nu	Sh
(a) Da = 10^{-2}	100×100	5.7910	6.9206	9.4549
	150×150	5.7888	6.7603	9.2405
	200×200	5.8003	6.7312	9.2069
	300×300	5.7857	6.6550	9.1136
	400×400	5.7723	6.6133	9.0978
(a) Da = 10^{-3}	100×100	4.2589	6.2420	8.7135
	150×150	4.2710	6.1008	8.5341
	200×200	4.2759	6.0793	8.5056
	300×300	4.2733	6.0171	8.4340
	400×400	4.2694	5.9839	8.4019
(a) Da = 10^{-4}	100×100	1.6077	4.5162	5.6569
	150×150	1.6243	4.3985	5.5388
	200×200	1.6272	4.3879	5.5321
	300×300	1.6313	4.3409	5.4852
	400×400	1.6315	4.3339	5.4596
(b) Da = 10^{-4}	100×100	9.5747	11.0417	31.4131
	200×200	9.7174	10.7197	31.1201
	400×400	9.7835	10.6325	30.9089
(b) Da = 10^{-5}	100×100	3.2643	6.0646	22.0111
	200×200	3.3252	5.9701	21.4933
	400×400	3.3438	5.9023	21.2571
(b) Da = 10^{-6}	100×100	0.6041	4.0617	8.5908
	200×200	0.6398	3.9491	8.6692
	400×400	0.6409	3.8912	8.7259

400×400, the maximum relative difference registered stays below 1.3%. Therefore, the grid 200×200 was judged enough to conduct the present study.

4 Results and Discussion

The numerical code developed for the present investigation has been used to carry out.

a number of simulations for a wide range of controlling parameters such as buoyancy ratio N, thermal Rayleigh number Ra_T, Darcy number Da, Lewis number Le, and the porosity of the porous medium ε, varying, respectively, in the ranges $-5 \leq N \leq 5$, $10^4 \leq Ra_T \leq 10^7, 10^{-6} \leq Da \leq 10^{-2}, 1 \leq Le \leq 10$ and $0.4 \leq \varepsilon \leq 0.8$.

4.1 Effect of Thermal Rayleigh Number

The effect of thermal Rayleigh number on streamlines, isotherms, and iso-concentration patterns is shown in Fig. 4 for Le = 2.0, $N = 5.0$, $\varepsilon = 0.4$ and Da = 10^{-4}. It is observed that all these distributions are characterized by perfect symmetry with respect to the vertical median of the cavity. This behavior results from the symmetry of the configuration and the imposed boundary conditions with respect to this axis. Regarding the overall

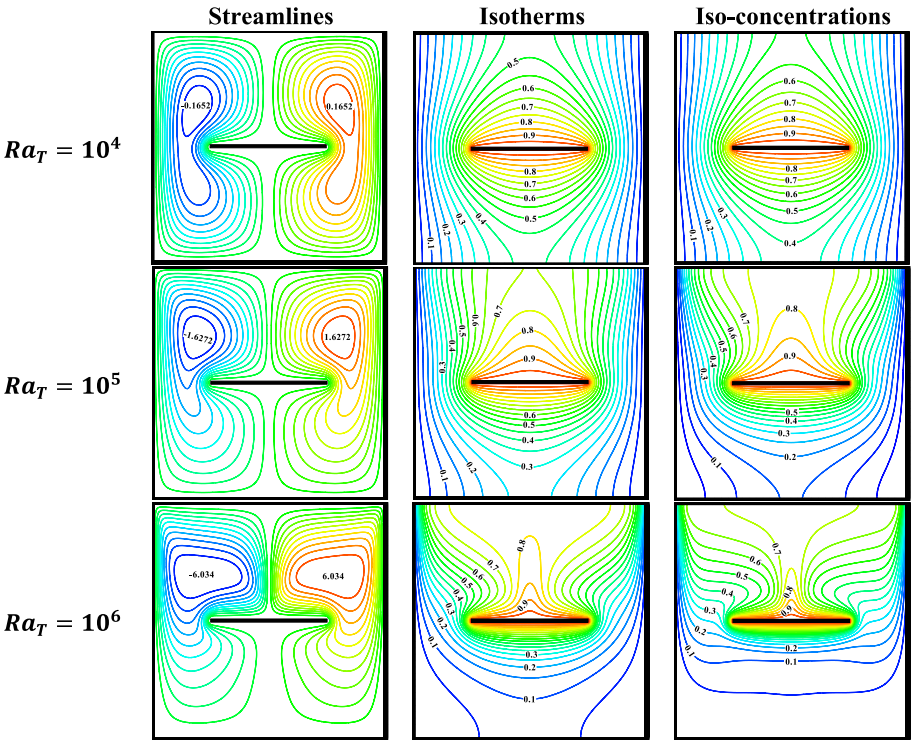

Fig. 4 Effect of Rayleigh number on streamlines, isotherms, and iso-concentrations for Le = 2.0, $N = 5.0$, and Da = 10^{-4}

behavior, the streamlines indicate the presence of two symmetrical counter-rotating cells both rising at the mid-width of the cavity and falling along the vertical cold walls due to the buoyancy effect. The upward movement of the cells is imposed by the buoyancy forces resulting from the heating ensured by the heated plate. As a result, the cells cores (i.e., positions of ψ_{max} and ψ_{min}) are located above the latter plate**.** In fact, under the effect of thermal buoyancy forces, the hot fluid near the upper face of the plate is driven upwardly on either side of the vertical median plane, leading to the generation of a clockwise cell on the right side of the cavity and a counterclockwise one on its left side. More specifically, for this case corresponding to aiding buoyancy forces and $N = 5$, heat and mass transfer are mainly dominated by the diffusive effect at $Ra_T = 10^4$, while convection plays a limited role. The increase of thermal Rayleigh number above this value leads to a more important increase in the flow intensity above the heated plate taking advantage of its destabilizing effect (the heated plate ensuring a heating from below for the upper half of the cavity), which results in a remarkable disproportionality in the magnitude and the distribution of the flow velocity between the upper and lower halves of the cavity. In parallel, the increase of Ra_T promotes the intensification of both cells by a factor of 36.5 (from $\psi_{max} = 0.1652$ to $\psi_{max} = 6.034$) by augmenting Ra_T from 10^4 to 10^6.

Concerning the thermal aspect of the problem, the examination of the isotherms of Fig. 4 indicates that the thermal Rayleigh number has a considerable impact on the distribution of the temperature field. The isotherms are also symmetrical with respect to the

vertical median plane of the cavity. At low thermal Rayleigh number ($Ra_T = 10^4$), the isotherms are vertical lines slightly deformed near the vertical walls and become more and more curved while moving toward the hot plate. Globally, the conductive regime is dominant for this relatively low value of Ra_T as evidenced by the distribution of the isotherms resulting from the imposed thermal conditions. The increase of Ra_T leads to a progressive establishment of vertical thermal boundary layers near the upper parts of the cold walls and contributes to the formation of a plume just above the central part of the heated plate when the convective effects prevail (case of $Ra_T = 10^6$). Thus, the distribution of the isotherms is obviously affected by the increase of Ra_T. Consequently, in the presence of the thermal plume above the heated plate, the heat transfer between the fluid and the heated plate is enhanced accordingly. However, in the lower half of the cavity (beneath the heated plate), conduction stays the dominant mode regardless of the Rayleigh value; it corresponds to a case of a region heated from above and cooled laterally.

Figure 4 shows that the iso-concentration distributions exhibit a kind of resemblance with the isotherms, and they are also characterized by the appearance of a solutal plume above the heated plate for $Ra_T = 10^6$. Due to the fact that $Le > 1$, the thermal diffusive effect prevails over the solutal diffusive one, which leads to solutal plume thinner compared to the thermal one. In addition, the increase of Ra_T engenders solutal gradients stronger than the thermal ones near the upper parts of the vertical walls and around the heated plate.

4.2 Effect of Darcy Number

The effect of Darcy number Da is exemplified in terms of streamlines, isotherms, and iso-concentration patterns for $Le = 2.0$ and $\varepsilon = 0.4$. For $Ra_T = 10^5$ and $N = 5.0$, Fig. 5 illustrates this effect in the range $10^{-4} \leq Da \leq 10^{-2}$, while for $Ra_T = 10^7$ and $N = 1.0$, this effect is illustrated in Fig. 6 for Da varying in the range $10^{-6} \leq Da \leq 10^{-4}$. It should be noted that the decrease in the Darcy number increases the resistance of the porous matrix to fluid flow, which leads to an attenuation of the convective transports. Thus, Fig. 5 shows that, by decreasing the Darcy number from 10^{-4} to 10^{-2}, the flow intensity undergoes an intensification by a factor of about 256%. The flow strengthening may be explained by the increase in the modified Rayleigh number $Ra_m = Ra_T \times Da$. At $Da = 10^{-4}$, the reduced flow intensity and the low heat transfer between the heated plate and the surrounding fluid lead to large thermal plumes above the heated plate, while beneath the latter, the vertical thermal gradients decrease downward expressing a dominance of the diffusive regime. The interaction between the working fluid and the cold walls is noteworthy, but the thermal boundary layers are relatively thick in the areas where the horizontal thermal gradients are the most important. The increase in Darcy number is accompanied by an intensification of the flow intensity and the formation of sharper thermal and solutal plumes above the heated plate. Consequently, heat and mass transfers between the working fluid and the active boundaries are accentuated, which leads to a reduction of the thermal and solutal boundary layers' thicknesses near the upper parts of the cold walls. The important distortions exhibited by the isotherms and iso-concentration in the region located above the extremities of the heated plate when Da is increased from 10^{-4} to 10^{-2} evidences that the increase of the porous matrix permeability enhances strongly the convective transports within the cavity**.** Finally, by increasing Darcy number, the temperature and concentration boundary layers around the heated plate become thinner, which results in stronger heat and mass transfer abilities.

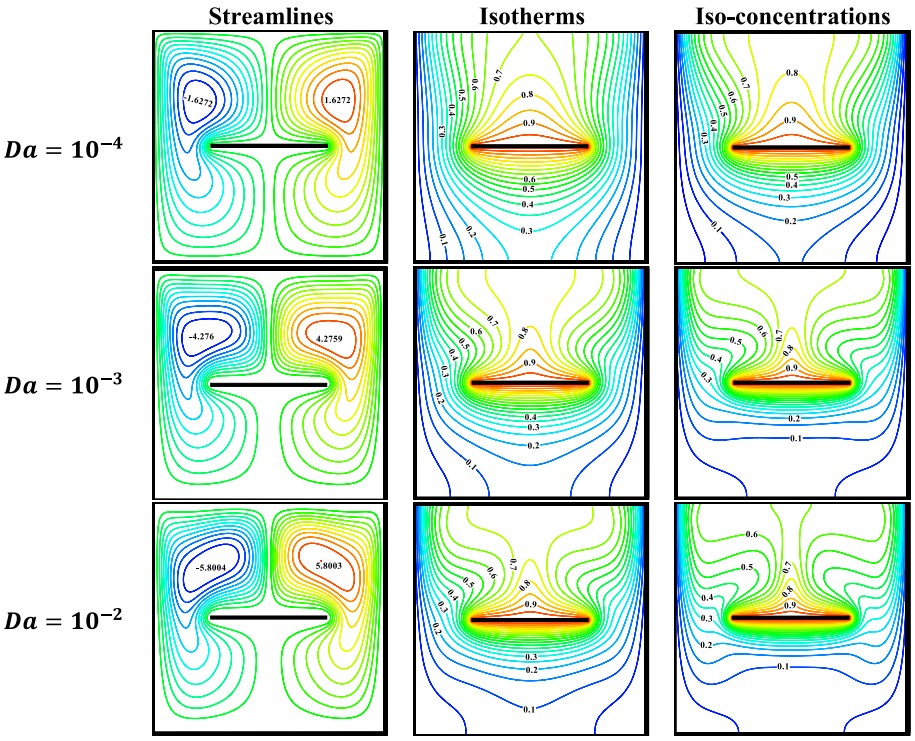

Fig. 5 Effect of Darcy number on streamlines, isotherms, and iso-concentrations for Le = 2.0, $N = 5.0$, and $Ra_T = 10^5$

By augmenting Ra_T to 10^7 and considering the ratio of the solutal and thermal buoyancy forces equal to unity ($N = 1$), the global behaviors stay similar. The heat and mass transfers are, as expected, promoted by this increase in Rayleigh number, and these increase all the more as the permeability (Darcy number) rises. In fact, as it can be seen in Fig. 6, the flow intensity undergoes an abrupt augmentation of about 1481% when Darcy number is incremented from 10^{-6} to 10^{-4}. Following the increase in Darcy number, the intensification of the flow leaving the lower half of the cold/(less concentrated) walls leads to an extension of the cold zone /(low concentration zone) created in the vicinity of the lower horizontal boundary. For this high value of Ra_T, the thermal and solutal plumes above the heated plate are more marked than those observed for the case $Ra_T = 10^5$ and Da = 10^{-4}.

By setting $Ra_T = 10^7$, $N = 1$ and increasing the value of the Lewis number to Le = 10, the flow intensity undergoes a noticeable drop at a given Darcy number. As a result, the diffusion of heat is faster than that of species leading to thicker thermal boundary layers compared to the solutal ones as evidenced by the isotherms and iso-concentrations in Fig. 7. Moreover, above the heated plate, the solutal plumes are more asserted than the thermal ones and beneath its iso-concentrations are denser, improving by the way the ability of dimensionless mass transfer. These behaviors are amplified by increasing the permeability of the porous matrix through the Darcy number (the porosity being considered constant).

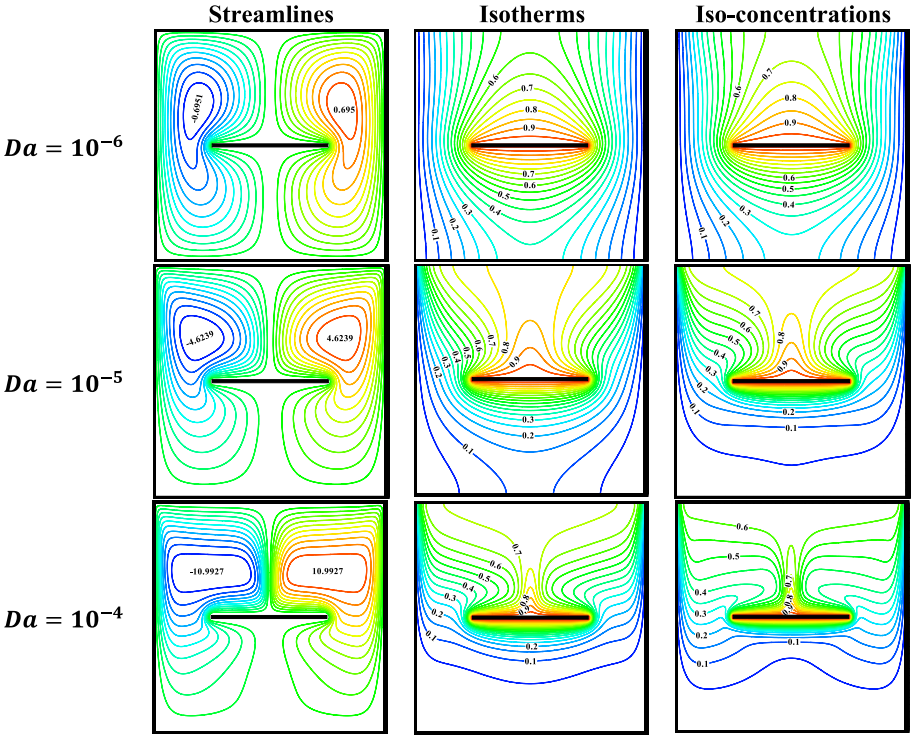

Fig. 6 Effect of Darcy number on streamlines, isotherms, and iso-concentrations for Le = 2.0, $N = 1.0$, and $\mathrm{Ra_T} = 10^7$

4.3 Effect of Buoyancy Ratio

The effect of the buoyancy ratio N is illustrated in Fig. 8 for N varying in the range $-5 \leq N \leq 5$ to cover the cases of aiding and counteracting buoyancy forces. This effect is illustrated in terms of streamlines, isotherms, and iso-concentrations for Le = 2.0, $\mathrm{Ra_T} = 10^5$, $\mathrm{Da} = 10^{-3}$ and $\varepsilon = 0.4$. It should be noted that the buoyancy ratio characterizes the relative magnitudes of the thermal and solutal buoyancy forces. A negative value of N means that buoyancy forces due to heat and mass transfer act in opposite directions, which leads to an opposing mode. On the contrary, a positive value of N means that these forces are acting in the same direction and the corresponding mode is an aiding one. The particular value $N = 0$ (pure thermal case) corresponds to a situation for which the buoyancy solutal force is canceled. Then, the flow within the cavity is driven solely by the imposed thermal conditions. A close inspection of the streamlines in Fig. 8 shows that the variation of the parameter N leads to important qualitative and quantitative changes in the flow structure, but the symmetry with respect to the vertical mid-plane is preserved. In fact, for the negative values of N, the left cell is clockwise rotating while the right one is counterclockwise and their cores are located beneath the heated plate. Thus, the direction of cell rotation is imposed by the solutal force. The increment of N from its lower value reduces the intensity of the cells since it leads to a weakening of the solutal buoyancy force. For the case of equal but opposite buoyancy forces ($N = -1$), the flow cell intensities

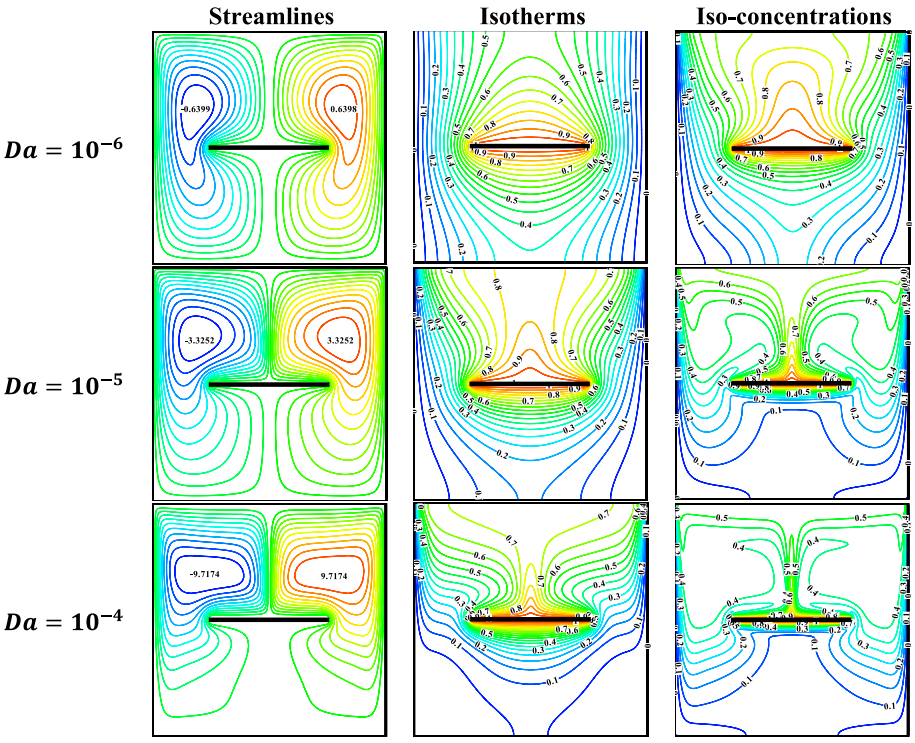

Fig. 7 Effect of Darcy number on streamlines, isotherms, and iso-concentrations for Le = 10, $N = 1.0$, and $\mathrm{Ra_T} = 10^7$

are considerably attenuated due to the strong competition between the solutal and thermal buoyancy forces. This competition between the buoyancy forces is not existing for $N = 0$, allowing the thermal buoyancy force to control the flow. The solutal force plays a supportive role for $N > 0$, which leads to a better accentuation of the flow intensity by increasing N in its positive range. More specifically, for $N = 5$, the flow is about 25% more intense than that generated for $N = -5$ and its intensity is multiplied by a factor of 2.5 when the value of N goes from 0 to 5. This important intensification results from the aiding effects of the thermal and solutal buoyancy forces that act together to promote the fluid circulation. The locations of the extremums values of ψ are symmetrically situated above the heated plate as stated before for $N \geq 0$.

Due to the strong coupling between the governing equations, the thermal and solutal aspects of the problem are also seen to be very sensitive to the variations of N. Thus, the thermal and solutal plumes are located below the heated plate and oriented downward for $N = -5$, while their locations are above the plate, and they are facing upward for $N \geq 0$. In addition, the areas of high thermal and solutal gradients are located near the lower parts of the cold walls for dominant solutal forces acting opposite to the thermal ones. Globally, the solutal thermal gradients are higher than the thermal ones when the solutal forces are dominant. For the case corresponding to equal but opposite thermal and solutal buoyancy forces ($N = -1$), the role played by Le becomes negligible since the diffusive regime prevails (the flow intensity being strongly attenuated) as shown by

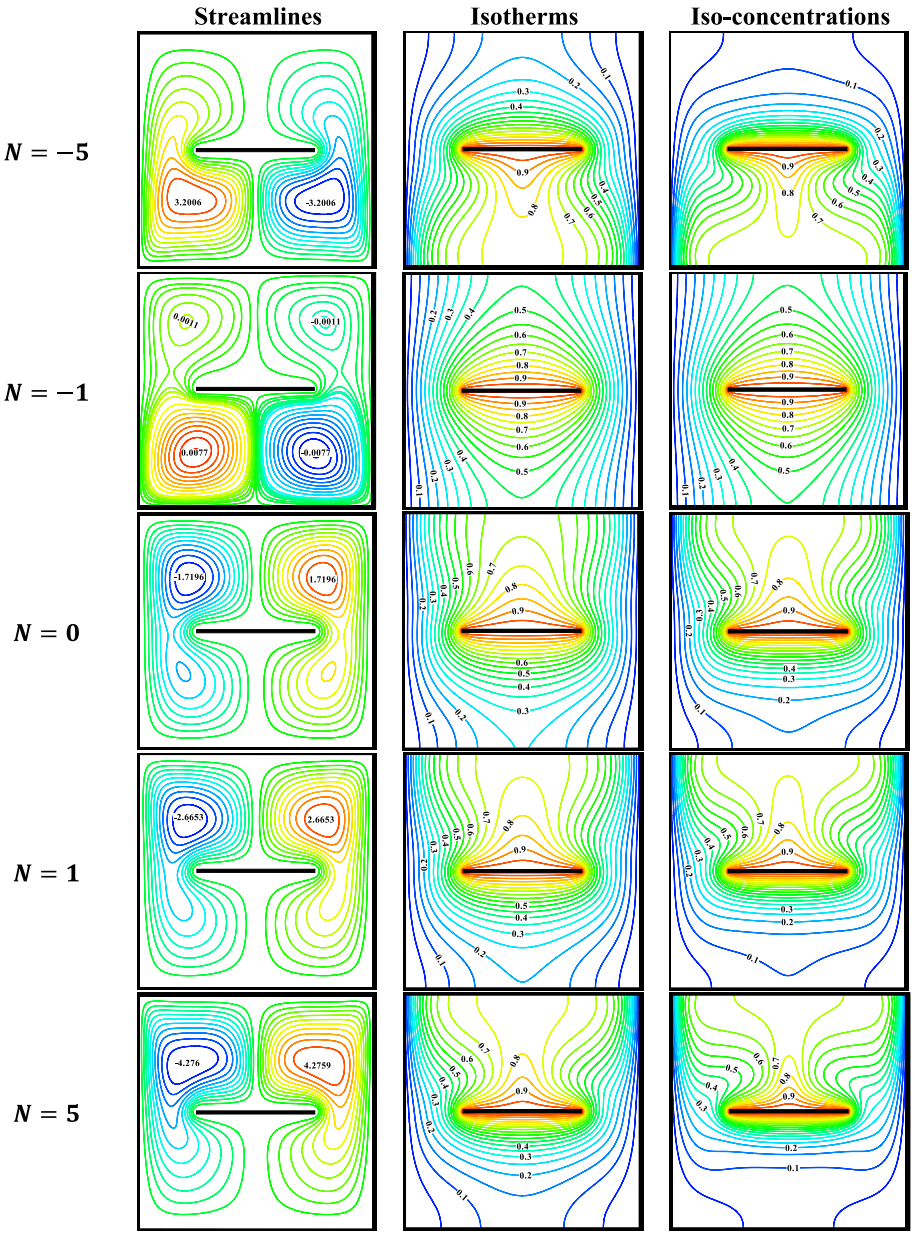

Fig. 8 Effect of buoyancy ratio on streamlines, isotherms, and iso-concentrations for Le = 2.0, Da = 10^{-3}, and $Ra_T = 10^5$

the distribution of the isotherms and the iso-concentrations. The latter are characterized by a quasi-double symmetry: a symmetry with respect to the vertical mid-plane and a quasi-symmetry with respect to the heated plate.

4.4 Effects of Lewis Number

Streamlines, isotherms, and iso-concentrations are presented in Fig. 9 to illustrate the effect of the Lewis number for Da = 10^{-3}, $N = 1.0$, $\varepsilon = 0.4$ and $\mathrm{Ra_T} = 10^5$. It can be noticed that the symmetry of the solutions with respect to the vertical mid-plane is not affected by the increase in the Lewis number. In addition, for Le = 1, the temperature and concentration fields are identical because of the equality of the thermal and solutal diffusivities. By increasing the Lewis number from 1 to 10, the flow intensity undergoes a decrease of about 34%, while the distribution of the isotherms is barely affected by this increase. In fact, the temperature distribution is rather affected by the changes of velocity and the latter is controlled by the Rayleigh number and the buoyancy ratio that are maintained constant. The limited changes observed on the distribution of the isotherms result from the flow intensity changes accompanying the increase of Le. Moreover, the increase of Le from 1 to 10 leads

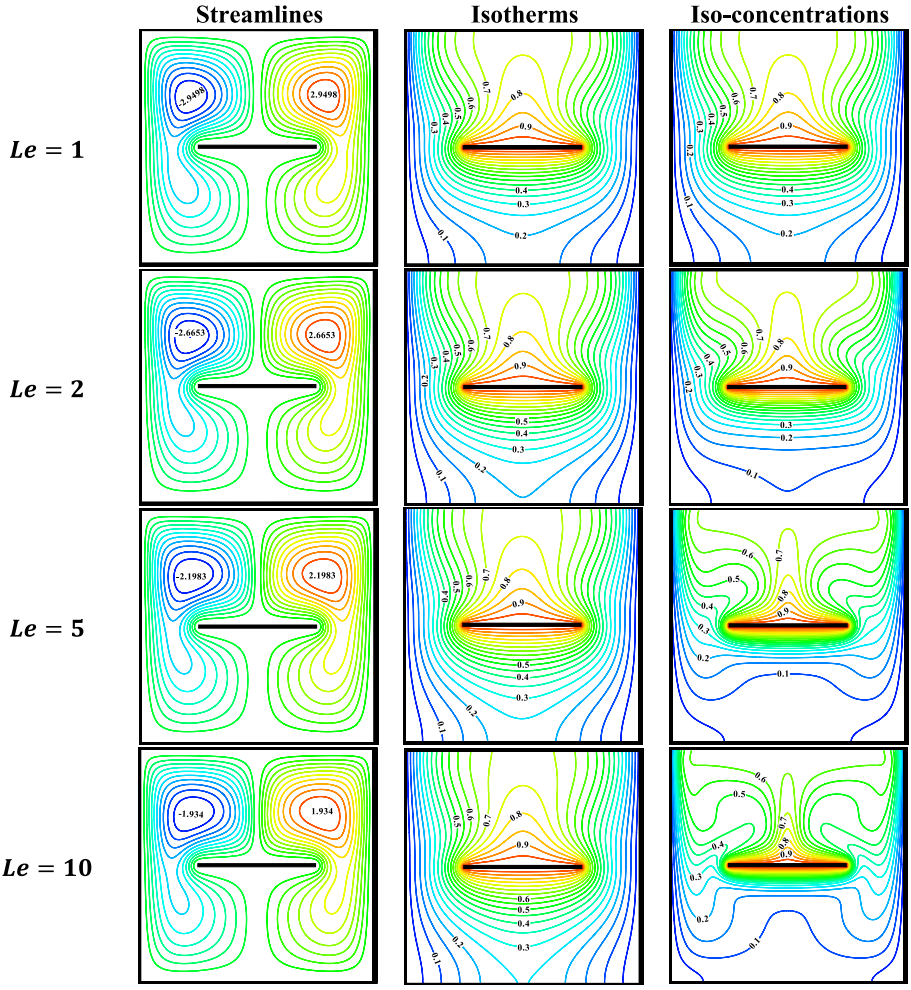

Fig. 9 Effect of Lewis number on streamlines, isotherms, and iso-concentrations for $N = 1.0$, Da = 10^{-3}, and $\mathrm{Ra_T} = 10^5$

to an increase of the solutal Rayleigh number by a factor of 10, which favors the solutal plume above the heated plate and makes the iso-concentrations denser around the latter and the solutal boundary layers thinner near the upper parts of the cold walls.

4.5 Average Nusselt and Sherwood Numbers

Variations versus the Lewis number Le, of the average Nusselt and Sherwood numbers, are presented, respectively, in Fig. 10a, b for $\varepsilon = 0.4$, $N = 1$, $Ra_T = 10^5$ and various values of Da. Regarding the overall behavior, Fig. 10a shows that for a medium with weak permeability, the Nusselt number is quasi-insensitive to the variations of Le; it decreases very slightly and linearly toward an asymptotic limit around Nu = 3.9. Concretely, that means that heat transfer is not affected by the diffusive property of the solute in the porous medium for the considered value of Ra_T. For relatively large values of Da (case illustrated here with $Da = 10^{-3}$ and 10^{-2}), Nu decreases nonlinearly with the Lewis number. This behavior is compatible with the decrease in the flow intensity accompanying the increment of Le in Fig. 9. In addition, Fig. 10 shows also an increase of Nu by increasing Da since the porous matrix becomes more permeable and allows an intensification of the flow cells due to the effective increase in the porous Rayleigh number.

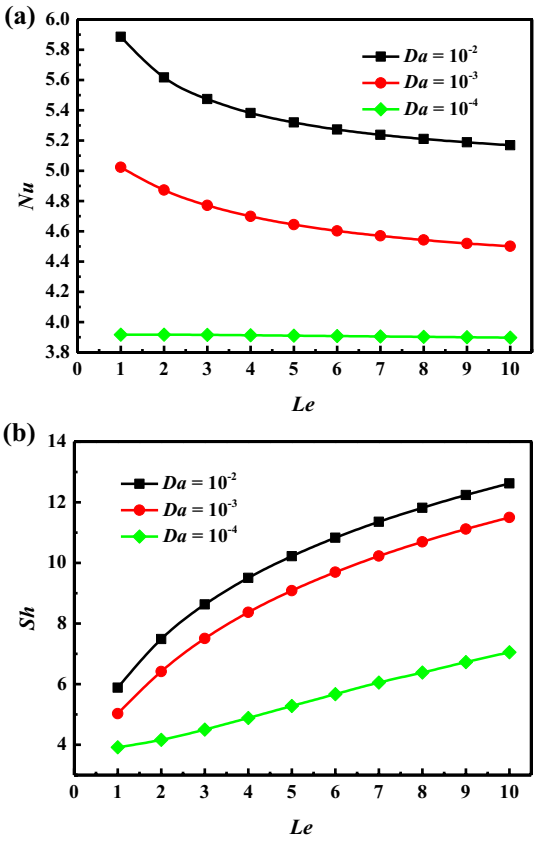

Fig. 10 Variations of the average Nusselt number (**a**) and Sherwood number (**b**) versus the Lewis number for $N = 1$ and $Ra_T = 10^5$

The variation of Sherwood number versus Le, exemplified in Fig. 10b is characterized by a quasi-linear increase for Da = 10^{-4} and nonlinear monotonous increase for the remaining values of Da. In fact, the increase of Sh accompanying the increment of Le, for a given Da, is attributed to the resulting increase in the solutal Rayleigh number. In addition, for a given Le, both Nu and Sh are supported by the increase in the Darcy number; behavior is explained by a reduction of the porous matrix resistance to fluid motion (increase of the medium permeability, allowing better fluid circulation). For instance, the quantification of the increase of Nu/(Sh) for Le = 5 is about 36% /(94%) when Darcy number goes from 10^{-4} to 10^{-2}.

Variations versus the Buoyancy ratio N, of the average Nusselt and Sherwood numbers, are illustrated, respectively, in Fig. 11a, b for $\varepsilon = 0.4$, Le = 2, $\mathrm{Ra_T} = 10^5$ and various values of Da. It can be seen that both Nu and Sh variations versus N are characterized by similar tendencies. More precisely, for each value of Da, Fig. 11 shows monotonous and similar decreases of Nu and Sh when N increases from -5 to -1, followed by monotonous augmentations when N increases in the remaining range. The rates of increase and decrease of Nu and Sh depend obviously on Da. The common decrease of these quantities in the range $-5 \leq N \leq -1$ is attributed to the reduction of the solutal buoyancy force in favor of an increasing competition effect on the part of the thermal one. This competition between the latter reaches its limit at $N = -1$ when they become equally intense with opposite effects.

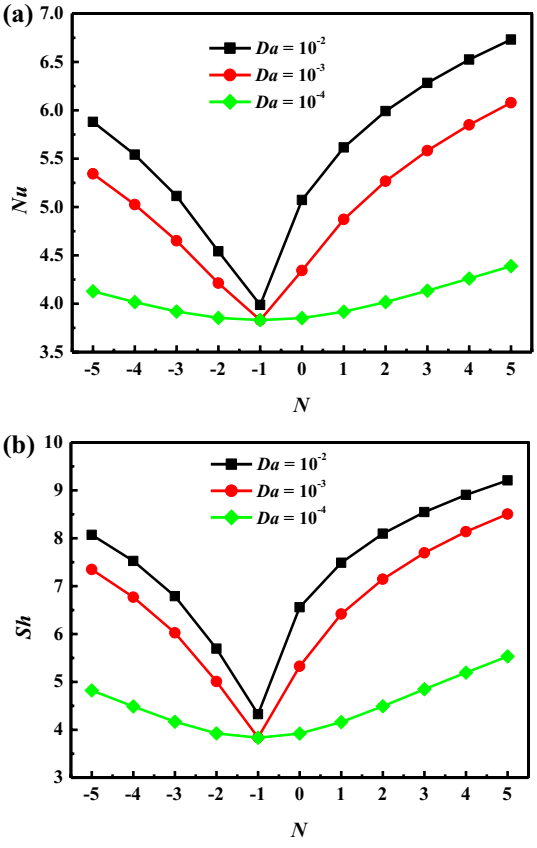

Fig. 11 Variations of the average Nusselt number (**a**) and Sherwood number (**b**) versus the buoyancy ratio for Le = 2 and $\mathrm{Ra_T} = 10^5$

Thus, the minimum heat and mass transfer occurring at $N = -1$ results from the maximum antagonist effect of the solutal and thermal buoyancy forces that also considerably slows down the flow intensity. The change in trends from $N = -1$ is a consequence of the cooperating role of the buoyancy forces that leads to an improvement in terms of Nu and Sh with faster rates in the remaining range of N.

More details on the effect of Darcy number on Nu and Sh are provided in Fig. 12 for $N = 1$, $\mathrm{Ra_T} = 10^5$, $\varepsilon = 0.4$ and various values of Le. At $\mathrm{Da} = 10^{-4}$, Fig. 12a shows that Nu is almost not affected by the increase of Le (results corroborated by Fig. 10a), while Sh is more sensitive to the latter variation; it increases by increasing Le. The increase in Darcy number in the range $Da \leq 2 \times 10^{-3}$ leads to a fast increase in Nu and Sh with Le. Thus, for high values of permeability, both heat and mass transfers tend toward constant values that depend on Le. Note also that for a given Da, Nu and Sh show opposite tendencies by increasing Le.

Further additional information on the combined effect of Rayleigh and Darcy numbers on Nu and Sh is presented in Table 5 for various values of the porosity ($0.4 \leq \varepsilon \leq 0.8$), $\mathrm{Le} = 2$, $\mathrm{Ra_T}$ ranging from 10^4 to 10^6 and $N = 5$. For given Rayleigh number and porosity, the Darcy number may be varied through the permeability and its increase (through the permeability) has a positive impact on average Nusselt and Sherwood numbers. In fact, a more permeable medium allows easier fluid circulation, resulting in a higher flow

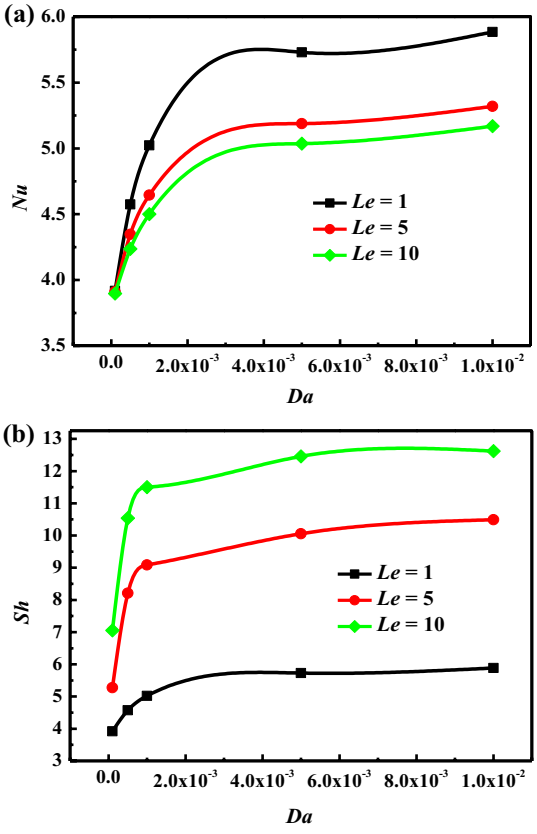

Fig. 12 Variations of the average Nusselt number (**a**) and Sherwood number (**b**) versus Darcy number for $N = 1$ and $\mathrm{Ra_T} = 10^5$

Table 5 Average Nusselt and Sherwood numbers for Le = 2 and $N = 5$, and different values of Ra_T, ε, and Da

	Ra_T	Da	Nu	Sh
$\varepsilon = 0.4$	10^4	10^{-2}	4.4232	5.4370
		10^{-3}	4.0306	4.5475
		10^{-4}	3.8270	3.8596
	10^5	10^{-2}	6.7312	9.2069
		10^{-3}	6.0793	8.5056
		10^{-4}	4.3879	5.5321
	10^6	10^{-3}	10.2692	14.3846
		10^{-4}	8.2894	12.2527
		10^{-5}	4.6284	6.1494
$\varepsilon = 0.6$	10^4	10^{-2}	4.6903	5.9605
		10^{-3}	4.0989	4.7454
		10^{-4}	3.8280	3.8628
	10^5	10^{-2}	7.4334	10.1957
		10^{-3}	6.5885	9.3288
		10^{-4}	4.4548	5.7081
	10^6	10^{-3}	11.4397	15.9693
		10^{-4}	8.8787	13.1952
		10^{-5}	4.6655	6.2635
$\varepsilon = 0.8$	10^4	10^{-2}	4.9096	6.3696
		10^{-3}	4.1497	4.8898
		10^{-4}	3.8287	3.8650
	10^5	10^{-2}	7.9701	10.9334
		10^{-3}	6.9556	9.9131
		10^{-4}	4.4972	5.8182
	10^6	10^{-3}	12.2863	17.1333
		10^{-4}	9.2676	13.8274
		10^{-5}	4.6879	6.3149

intensity and thereby more important heat and mass transfers. This increase is evidently promoted by augmenting Ra_T. For example, for $Ra_m = Ra_T \times Da = 100$ and $\varepsilon = 0.4$, Nu /(Sh) undergoes an improvement of about 87.4%/(125%) when Ra_T rises from 10^4 to 10^6.

Regarding the porosity of the porous medium, its effect is also significant. In fact, Table 5 shows, for instance, that, for $Ra_T = 10^6$ and $Da = 10^{-3}$, Nu/(Sh) undergoes an improvement of about 19.6%/19.10% when the porosity ε is augmented from 0.4 to 0.8.

As regards the combined effect of the Lewis and Darcy numbers on Nu and Sh, the results presented in Table 6 for $\varepsilon = 0.4$, $Ra_T = 10^7$, $N = 1$ and different Da so that the modified Rayleigh number $Ra_m = Ra_T \times Da \leq 10^3$, illustrate clearly this effect. As it can be seen in Table 6, for a fixed modified Rayleigh number Ra_m, the increase in the value of the Lewis number leads to a reduction in the rate of heat transfer and an important improvement in the rate of mass transfer. For example, for $Ra_m = 1000$, Nu decreases by 12.10%, while Sh undergoes an improvement of 80.50% when Le increases from 2 to 10.

Table 6 Average Nusselt and Sherwood numbers for $Ra_T = 10^7$, $\varepsilon = 0.4$, $N = 1$ and different values of Le and Da

Le	Da	Nu	Sh
2	10^{-4}	12.1922	17.2377
	10^{-5}	7.0499	10.6790
	10^{-6}	3.9744	4.3325
10	10^{-4}	10.7197	31.1201
	10^{-5}	5.9701	21.4933
	10^{-6}	3.9491	8.6692

In addition, the increase of Le is seen to have no significant effect on Nu for low Darcy numbers; behavior compatible with the results is presented in Sect. 4.4.

5 Conclusions

Double-diffusive natural convection in a porous cavity with heating and diffusing plate inside has been studied numerically using the multiple-relaxation-time lattice-Boltzmann method at the REV scale based on the generalized model. For Pr = 1, the combined effects of buoyancy ratio, N, thermal Rayleigh number, Ra_T, Darcy number, Da, Lewis number, Le, and the porosity ε of the porous medium on heat and mass transfers characteristics are investigated. The main results of this study are summarized as follows:

- The permeability of the porous medium, characterized by the Darcy number, significantly affects the flow and the distribution of isotherms and iso-concentrations in the porous cavity.
- Thermal and solutal plumes develop above/(below) the heated plate for $N > -1$/($N < -1$) and become prominent as the Darcy number increases, leading to improved heat and mass transfers. This improvement is supported by increasing Ra_T.
- For high values of the buoyancy ratio, whether positive or negative, double-diffusive natural convection is dominated by solutal volume force. At $N = -1$, the thermal and solutal buoyancy forces act in opposite directions and are equally intense. The resulting heat and mass transfers are particularly deteriorated for this particular case.
- The effect of the Lewis number on heat transfer is negligible for low Darcy values but leads to substantial variations in terms of Nu and Sh versus *Le* at relatively large Da.
- The increase of the porosity of the porous medium promotes the fluid flow intensity and heat and mass transfers in the cavity.

Funding There was no funding support for this study.

Declarations

Conflict of interest The authors declare that they have no known competing financial interests or personal relationships that could have appeared to influence the work reported in this paper.

References

Bejan, A.: Convection Heat Transfer, 4th edn. Wiley (2013)

Bennacer, R., Tobbal, A., Beji, H., Vasseur, P.: Double diffusive convection in a vertical enclosure filled with anisotropic porous media. Int. J. Therm. Sci. (2001). https://doi.org/10.1016/S1290-0729(00)01185-6

Benzi, R., Succi, S., Vergassola, M.: The lattice Boltzmann equation: theory and applications. Phys. Rep. **222**(3), 145–197 (1992)

Bergman, T.L., Incropera, F.P., Viskanta, R.: Correlation of mixed layer growth in a double-diffusive, salt-stratified system heated from below. J. Heat Transf. (1986). https://doi.org/10.1115/1.3246888

Carlsson, J.O.: Processes in interfacial zones during chemical vapour deposition: aspects of kinetics, mechanisms, adhesion and substrate atom transport. Thin Solid Films (1985). https://doi.org/10.1016/0040-6090(85)90358-X

Chamkha, A.J., Al-Naser, H.: Double-diffusive convection in an inclined porous enclosure with opposing temperature and concentration gradients. Int. J. Therm. Sci. (2001). https://doi.org/10.1016/S1290-0729(00)01213-8

Chen, F., Chen, C.F.: Double-diffusive fingering convection in a porous medium. Int. J. Heat Mass Transf. **36**, 793–807 (1993). https://doi.org/10.1016/0017-9310(93)80055-Y

Chen, S., Doolen, G.D.: Lattice Boltzmann method for fluid flows. Annu. Rev. Fluid Mech. (1998). https://doi.org/10.1146/annurev.fluid.30.1.329

Chen, X.B., Yu, P., Sui, Y., Winoto, S.H., Low, H.T.: Natural convection in a cavity filled with porous layers on the top and bottom walls. Transp. Porous Media (2009). https://doi.org/10.1007/s11242-008-9300-2

Coulter, J.P., Güçeri, S.I.: Laminar and turbulent natural convection in solar energy applications. In: Yüncü, H., Paykoc, E., Yener, Y. (eds.) Solar Energy Utilization, pp. 303–333. Springer Netherlands, Dordrecht (1987)

Dahani, Y., Hasnaoui, M., Amahmid, A., Hasnaoui, S.: A Multiple-Relaxation-Time lattice Boltzmann analysis of coupled mixed convection and radiation effect in a tilted two-sided lid-driven enclosure. Chem. Phys. Lett. **791**, 139386 (2022). https://doi.org/10.1016/j.cplett.2022.139386

de Ferrières, S., El Bakali, A., Gasnot, L., Montero, M., Pauwels, J.F.: Kinetic effect of hydrogen addition on natural gas premixed flames. Fuel **106**, 88–97 (2013). https://doi.org/10.1016/j.fuel.2012.06.045

El Bakali, A., Mercier, X., Wartel, M., Acevedo, F., Burns, I., Gasnot, L., Pauwels, J.-F., Desgroux, P.: Modeling of PAHs in low pressure sooting premixed methane flame. Energy **43**, 73–84 (2012). https://doi.org/10.1016/j.energy.2011.12.026

Ergun, S.: Fluid flow through packed columns. Chem. Eng. Prog. **48**, 89–94 (1952)

Gao, D., Chen, Z., Chen, L.: A thermal lattice Boltzmann model for natural convection in porous media under local thermal non-equilibrium conditions. Int. J. Heat Mass Transf. (2014). https://doi.org/10.1016/j.ijheatmasstransfer.2013.11.050

Gong, S., Cheng, P.: Lattice Boltzmann simulation of periodic bubble nucleation, growth and departure from a heated surface in pool boiling. Int. J. Heat Mass Transf. (2013). https://doi.org/10.1016/j.ijheatmasstransfer.2013.03.058

Guo, Z., Zhao, T.S.: Lattice Boltzmann model for incompressible flows through porous media. Phys. Rev. E Stat. Phys. Plasmas Fluids Relat. Interdiscip. Top. (2002). https://doi.org/10.1103/PhysRevE.66.036304

Hasnaoui, S., Amahmid, A., Raji, A., Beji, H., El Mansouri, A., Hasnaoui, M.: LBM simulation of stabilizing/destabilizing effects of thermodiffusion and heat generation in a rectangular cavity filled with a binary mixture. Int. Commun. Heat Mass Transf. (2021). https://doi.org/10.1016/j.icheatmasstransfer.2021.105417

Howell, J.R., Hall, M.J., Ellzey, J.L.: Combustion of hydrocarbon fuels within porous inert media. Prog. Energy Combust. Sci. (1996). https://doi.org/10.1016/0360-1285(96)00001-9

Kaisare, N.S., Vlachos, D.G.: A review on microcombustion: fundamentals, devices and applications. Prog. Energy Combust. Sci. **38**, 321–359 (2012). https://doi.org/10.1016/j.pecs.2012.01.001

Kang, Q., Zhang, D., Chen, S.: Unified lattice Boltzmann method for flow in multiscale porous media. Phys. Rev. E Stat. Phys. Plasmas Fluids Relat. Interdiscip. Top. (2002). https://doi.org/10.1103/PhysRevE.66.056307

Kang, Q., Lichtner, P.C., Zhang, D.: An improved lattice Boltzmann model for multicomponent reactive transport in porous media at the pore scale. Water Resour. Res. (2007). https://doi.org/10.1029/2006WR005551

Karimi-Fard, M., Charrier-Mojtabi, M.C., Vafai, K.: Non-darcian effects on double-diffusive convection within a porous medium. Numer. Heat Transf. Part A Appl. (1997). https://doi.org/10.1080/10407789708914067

Khair, K.R., Bejan, A.: Mass transfer to natural convection boundary layer flow driven by heat transfer. J. Heat Transf. **107**, 979–981 (1985). https://doi.org/10.1115/1.3247535

Liu, Q., He, Y.L.: Multiple-relaxation-time lattice Boltzmann model for simulating double-diffusive convection in fluid-saturated porous media. Int. J. Heat Mass Transf. (2018). https://doi.org/10.1016/j.ijheatmasstransfer.2017.12.155

Liu, Q., He, Y.L., Li, Q., Tao, W.Q.: A multiple-relaxation-time lattice Boltzmann model for convection heat transfer in porous media. Int. J. Heat Mass Transf. (2014). https://doi.org/10.1016/j.ijheatmasstransfer.2014.02.047

Ma, Q., Chen, Z.: Numerical study on gas diffusion in isotropic and anisotropic fractal porous media (gas diffusion in fractal porous media). Int. J. Heat Mass Transf. (2014). https://doi.org/10.1016/j.ijheatmasstransfer.2014.08.064

Ma, Q., Chen, Z., Shi, J., Li, D.: Lattice Boltzmann modeling of VOC desorption and diffusion in porous materials. VOC desorption and diffusion. Build. Environ. (2014). https://doi.org/10.1016/j.buildenv.2013.11.011

Markham, B.L., Rosenberger, F.: Diffusive-convective vapor transport across horizontal and inclined rectangular enclosures. J. Cryst. Growth **67**, 241–254 (1984). https://doi.org/10.1016/0022-0248(84)90184-2

Mercier, X., Faccinetto, A., Batut, S., Vanhove, G., Božanić, D.K., Hróðmarsson, H.R., Garcia, G.A., Nahon, L.: Selective identification of cyclopentaring-fused PAHs and side-substituted PAHs in a low pressure premixed sooting flame by photoelectron photoion coincidence spectroscopy. Phys. Chem. Chem. Phys. **22**, 15926–15944 (2020). https://doi.org/10.1039/D0CP02740E

Mohamad, A.A., Bennacer, R., Azaiez, J.: Double diffusion natural convection in a rectangular enclosure filled with binary fluid saturated porous media: the effect of lateral aspect ratio. Phys. Fluids (2004). https://doi.org/10.1063/1.1630798

Mohamad, A.A.: Combustion in porous media. fundamentals and applications. In: Ingham, D.B., Pop, I.B.T.-T.P., P.M.I.I.I. (eds.) Transport Phenomena in Porous Media III, pp. 287–304. Pergamon, Oxford (2005)

Molla, M.M., Haque, M.J., Khan, M.A.I., Saha, S.C.: GPU Accelerated multiple-relaxation-time lattice Boltzmann simulation of convective flows in a porous media. Front. Mech. Eng. (2018). https://doi.org/10.3389/fmech.2018.00015

Mujeebu, M.A., Abdullah, M.Z., Bakar, M.Z.A., Mohamad, A.A., Abdullah, M.K.: Applications of porous media combustion technology—a review. Appl. Energy **86**, 1365–1375 (2009)

Mujeebu, M.A., Abdullah, M.Z., Mohamad, A.A., Bakar, M.Z.A.: Trends in modeling of porous media combustion. Prog. Energy Combust. Sci. **36**, 6274–6650 (2010)

Nield, D.A.: Onset of thermohaline convection in a porous medium. Water Resour. Res. (1968). https://doi.org/10.1029/WR004i003p00553

Nishimura, T., Imoto, T., Miyashita, H.: Occurrence and development of double-diffusive convection during solidification of a binary system. Int. J. Heat Mass Transf. (1994). https://doi.org/10.1016/0017-9310(94)90147-3

Nithiarasu, P., Seetharamu, K.N., Sundararajan, T.: Double-diffusive natural convection in an enclosure filled with fluid-saturated porous medium: a generalized non-darcy approach. Numer. Heat Transf. Part A Appl. (1996). https://doi.org/10.1080/10407789608913848

Nithiarasu, P., Seetharamu, K.N., Sundararajan, T.: Natural convective heat transfer in a fluid saturated variable porosity medium. Int. J. Heat Mass Transf. (1997a). https://doi.org/10.1016/S0017-9310(97)00008-2

Nithiarasu, P., Sundararajan, T., Seetharamu, K.N.: Double-diffusive natural convection in a fluid saturated porous cavity with a freely convecting wall. Int. Commun. Heat Mass Transf. (1997b). https://doi.org/10.1016/S0735-1933(97)00106-1

Saravanan, S., Sivaraj, C.: Coupled thermal radiation and natural convection heat transfer in a cavity with a heated plate inside. Int. J. Heat Fluid Flow. (2013). https://doi.org/10.1016/j.ijheatfluidflow.2013.01.007

Sathe, S.B., Tong, T.W., Faruque, M.A.: Experimental study of natural convection in a partially porous enclosure. J. Thermophys. Heat Transf. (1987). https://doi.org/10.2514/3.37

Seta, T., Takegoshi, E., Okui, K.: Lattice Boltzmann simulation of natural convection in porous media. Math. Comput. Simul. (2006). https://doi.org/10.1016/j.matcom.2006.05.013

Spaid, M.A.A., Phelan, F.R.: Lattice Boltzmann methods for modeling microscale flow in fibrous porous media. Phys. Fluids (1997). https://doi.org/10.1063/1.869392

Tang, G.H., Tao, W.Q., He, Y.L.: Gas slippage effect on microscale porous flow using the lattice Boltzmann method. Phys. Rev. E Stat. Nonlinear Soft Matter Phys. **5**, 1 (2005). https://doi.org/10.1103/PhysRevE.72.056301

Tasmin, M., Nag, P., Hoque, Z.T., Molla, M.M.: Non-Newtonian effect on heat transfer and entropy generation of natural convection nanofluid flow inside a vertical wavy porous cavity. SN Appl. Sci. (2021). https://doi.org/10.1007/s42452-021-04157-8

Trimis, D., Durst, F.: Combustion in a porous medium-advances and applications. Combust. Sci. Technol. (1996). https://doi.org/10.1080/00102209608935592

Vafai, K.: Convective flow and heat transfer in variable-porosity media. J. Fluid Mech. (1984). https://doi.org/10.1017/S002211208400207X

Viskanta, R.: Modeling of combustion in porous inert media. Spec. Top. Rev. Porous Media Int. J. **2**, 181–204 (2011). https://doi.org/10.1615/SpecialTopicsRevPorousMedia.v2.i3.30

Wang, L., Mi, J., Guo, Z.: A modified lattice Bhatnagar–Gross–Krook model for convection heat transfer in porous media. Int. J. Heat Mass Transf. (2016). https://doi.org/10.1016/j.ijheatmasstransfer.2015.11.040

Wood, S., Harris, A.T.: Porous burners for lean-burn applications, (2008)

Xu, H.T., Wang, T.T., Qu, Z.G., Chen, J., Li, B.B.: Lattice Boltzmann simulation of the double diffusive natural convection and oscillation characteristics in an enclosure filled with porous medium. Int. Commun. Heat Mass Transf. (2017). https://doi.org/10.1016/j.icheatmasstransfer.2016.12.001